IOP Publishing 2D Mater. 9 (2022) 044004 https://doi.org/10.1088/2053-1583/ac914c

2D Materials

RECEIVED
19 June 2022

REVISED
31 July 2022

ACCEPTED FOR PUBLICATION
12 September 2022

PUBLISHED
22 September 2022

PAPER

Electrically conductive porous $Ti_3C_2T_x$ MXene-polymer composites from high internal phase emulsions (HIPEs)

Huaixuan Cao[1], **Yifei Wang**[2], **Anubhav Sarmah**[1], **Kai-Wei Liu**[4], **Zeyi Tan**[2], **Kailash Dhondiram Arole**[2], **Jodie L Lutkenhaus**[1,2], **Miladin Radovic**[2], **Micah J Green**[1,2,*] and **Emily B Pentzer**[2,3,*]

[1] Artie McFerrin Department of Chemical Engineering, Texas A&M University, College Station, TX, United States of America
[2] Department of Materials Science and Engineering, Texas A&M University, College Station, TX, United States of America
[3] Department of Chemistry, Texas A&M University, College Station, TX, United States of America
[4] Texas A&M Transportation Institute, Texas A&M University, College Station, TX, United States of America
[*] Authors to whom any correspondence should be addressed.

E-mail: micah.green@tamu.edu and emilypentzer@tamu.edu

Keywords: conductive, porous, Ti_3C_2, MXene

Abstract

Porous MXene-polymer composites have gained attention due to their low density, large surface area, and high electrical conductivity, which can be used in applications such as electromagnetic interference shielding, sensing, energy storage, and catalysis. High internal phase emulsions (HIPEs) can be used to template the synthesis of porous polymer structures, and when solid particles are used as the interfacial agent, composites with pores lined with the particles can be realized. Here, we report a simple and scalable method to prepare conductive porous MXene/polyacrylamide structures via polymerization of the continuous phase in oil/water HIPEs. The HIPEs are stabilized by salt flocculated $Ti_3C_2T_x$ nanosheets, without the use of a co-surfactant. After polymerization, the polyHIPE structure consists of porous polymer struts and pores lined with $Ti_3C_2T_x$ nanosheets, as confirmed by scanning electron microscopy, energy dispersive x-ray spectroscopy, and x-ray photoelectron spectroscopy. The pore size can be tuned by varying the $Ti_3C_2T_x$ concentration, and the interconnected $Ti_3C_2T_x$ network allows for electrical percolation at low $Ti_3C_2T_x$ loading; further, the electrical conductivity is stable for months indicating that in these composites, the nanosheets are stable to oxidation at ambient conditions. The polyHIPEs also exhibit rapid radio frequency heating at low power (10 °C s^{-1} at 1 W). This work demonstrates a simple approach to accessing electrically conductive porous MXene/polymer composites with tunable pore morphology and good oxidation stability of the nanosheets.

1. Introduction

High internal phase emulsions (HIPEs) are concentrated emulsions with a volume fraction of the internal phase greater than 74% [1–3]. Commonly, surfactants are added into an aqueous phase containing hydrophilic monomers, oil is added, and oil-in-water HIPEs are formed by agitation of the mixture. The HIPEs can be used as templates to synthesize porous structures, i.e. polyHIPEs, by polymerization of the monomers in the continuous phase and subsequent removal of the dispersed phase. Radical polymerization is commonly used in polyHIPE formation, where an initiator is included in either the continuous or dispersed phase [4, 5]. Thus, in as prepared polyHIPEs, oil droplets are contained within a continuous polymer structure. By removing the oil, porous structures are obtained in which the pores are lined with the surfactant. The conditions used to form HIPEs and process the polyHIPEs dictate the pore size, interconnects, voids, and windows [6]. Due to their tunable pore morphology, permeability, and low density, polyHIPEs have been used in diverse applications, including gas adsorption [7], water treatment [8–10], catalyst supports [11], sensing [12, 13], and tissue engineering [14].

Conventional HIPEs are stabilized by small molecule surfactants, such as sodium dodecyl sulfate

[15] or cetyltrimethylammonium bromide (CTAB) [16], but in recent years, solid particles have gained increased attention for this purpose (e.g. Pickering HIPEs). Compared to small molecule surfactants, particle surfactants can lead to the formation of more stable emulsions, and also allow for the functional properties of the particles to be integrated into polyHIPEs. Polymer particles [17], silica particles [18], carbon nanotubes (CNTs) [19, 20], and graphene oxide (GO) nanosheets [21–26] have all been used as surfactants to prepare HIPEs and polyHIPEs. Among these, 2D nanosheets (e.g. GO) are of particular interest due to their high surface area and high aspect ratio. For example, Zheng *et al* reported the formation of polyHIPEs from water-in-oil HIPEs using the CTAB modified GO as the stabilizer [22]. In a similar vein, Yi *et al* studied the interconnectivity of porous poly(acrylic acid) polyHIPEs prepared from GO/CTAB stabilized oil-in-water Pickering HIPEs [21]. To integrate the favorable electrical properties of the particle surfactants into the materials produced, Yang *et al* prepared GO-lined polyHIPEs via polymerization of water-in-oil HIPEs, then reduced GO to rGO to make conductive porous structures for piezoresistive sensing [12]. Similarly, Woltornist *et al* utilized graphene sheets to stabilize water-in-oil HIPEs for the formation of conductive graphite composite polyHIPE foams [27].

A relatively new class of 2D nanomaterials is transition metal carbides, nitrides, or carbonitrides, collectively termed MXenes, first reported in 2011 [28]. These have been widely used in polymer composites, processed by, e.g. solution mixing or layer-by-layer assembly, but underutilized in HIPEs and polyHIPEs. The general chemical formula of MXenes is $M_{n+1}X_nT_x$ ($n = 1 - 3$), where the M is a transition metal, such as Ti or Nb, X is C or N, and T_x is the functional groups on the MXene surfaces (–OH, –O, –F). MXene nanosheets are synthesized from their parent MAX phase, $M_{n+1}AX_n$, where A is group 13 or 14 elements (e.g. Al), by selectively etching the A layer, followed by an exfoliation process [29, 30]. The abundant surface functionalities, high electrical conductivity, large surface area, and high catalytic activity render MXenes and their composites as emerging materials in energy storage [31–36], catalysis [37–39], sensing [40], and electromagnetic interference shielding [41–47].

Porous MXene polymer composites have been prepared by freeze drying [48–51], foaming [52–54], and depositing MXenes onto porous substrates [55–61]. For example, Xu *et al* synthesized a porous MXene/poly(vinyl alcohol) (PVA) foam by freeze drying a mixture of MXene and PVA from water, using ice as the template [51]. Li *et al* used a CO_2-assisted foaming strategy to prepare poly(vinylidene fluoride) (PVDF)/CNT/MXene composite foam. To do so, MXene, CNT, and PVDF were combined in an organic solvent and compression molding was used to make a film; then CO_2 was pumped into the composite in the autoclave to produce the composite foam [52]. In contrast, few studies focus on utilizing MXenes to stabilize HIPEs as a route to produce porous MXene/polymer composites. Bian *et al* used CTAB as a co-surfactant and concentrated $Ti_3C_2T_x$ nanosheets to form oil-in-water HIPEs and polymerized the water-soluble monomer 2-hydroxyethyl methacrylate to make porous $Ti_3C_2T_x$ polymer composites [62]. Alternatively, Fan and co-workers utilized an ionic liquid (3-hexadecyl-1-vinylimidazolium bromide) to assist in the formation of $Ti_3C_2T_x$ stabilized water-in-ionic liquid HIPEs; the ionic liquid phase was polymerized to produce $Ti_3C_2T_x$-containing polyHIPEs with high sensitivity in piezoresistive sensors [63]. Similarly, Zheng *et al* used the charged surfactant dihexadecyldimethylammonium bromide and $Ti_3C_2T_x$ nanosheets to fabricated electrically conductive porous $Ti_3C_2T_x$/polystyrene polyHIPEs from water-in-oil HIPEs [64]. In these examples, an organic co-surfactant was required for the $Ti_3C_2T_x$ nanosheets to stabilize the HIPEs, and was thus incorporated in the composites.

Herein, we report a simple and scalable method to prepare electrically conductive porous $Ti_3C_2T_x$/polyacrylamide composite polyHIPEs via polymerization of the continuous phase of oil-in-water HIPEs stabilized by salt-flocculated $Ti_3C_2T_x$ nanosheets, without the use of co-surfactants. As prior work in this area used co-surfactants, this is the first report of a MXene-only stabilized HIPE and polyHIPEs. To develop the HIPEs, we leveraged our previous report that NaCl can be used to overcome electrostatic repulsion and flocculate $Ti_3C_2T_x$ nanosheets so that they can stabilize oil-in-water Pickering emulsions [65]. As shown in scheme 1, the NaCl-flocculated $Ti_3C_2T_x$ nanosheets stabilize oil-in-water HIPEs, in which a monomer, crosslinker, and initiator were included in the continuous aqueous phase. $Ti_3C_2T_x$-containing polyHIPEs were obtained by polymerization of the monomer in the aqueous phase, washing to remove solvents, and drying under reduced pressure. A porous polymer structure with pores lined with $Ti_3C_2T_x$ nanosheets was expected and confirmed by scanning electron microscopy (SEM), energy dispersive x-ray spectroscopy (EDS), and x-ray photoelectron spectroscopy (XPS). The interconnected $Ti_3C_2T_x$-lined pores created an electrically conductive network in the polyHIPEs, and the samples showed excellent oxidation stability (i.e. consistent electrical conductivity over months of storage under ambient conditions). The $Ti_3C_2T_x$ polyHIPEs also showed high radio frequency (RF) heating of 10 $°C\ s^{-1}$ at low power (1 W), due

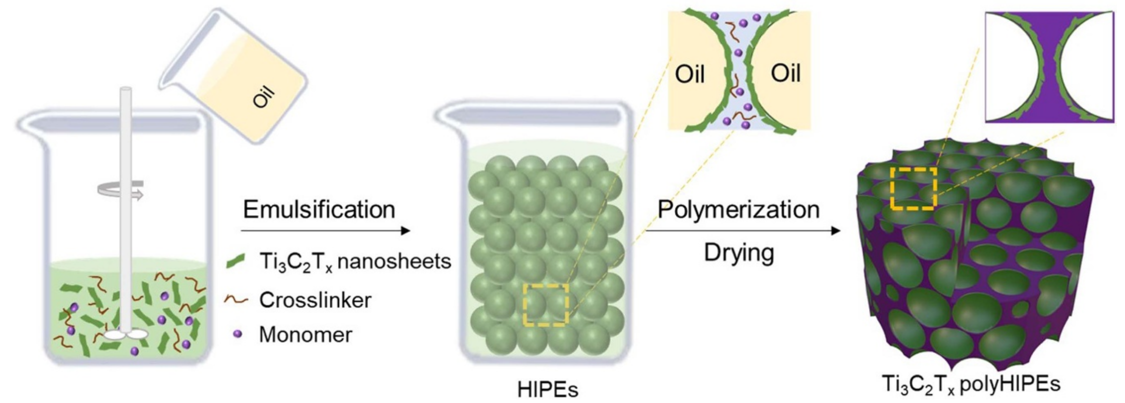

Scheme 1. Overview of the approach to preparing porous $Ti_3C_2T_x$-polymer composite polyHIPEs through polymerization of continuous phase in $Ti_3C_2T_x$ stabilized oil-in-water HIPEs.

to the interconnected conductive $Ti_3C_2T_x$ network. This work provides a simple approach to accessing conductive porous MXene-polymer composites with low loading of MXenes, high accessible surface area, tunable pore sizes, and oxidative stability. This route can be applied to other MXene (e.g. V- or Nb- based MXenes) and monomer compositions, providing a modular route to composite materials design.

2. Materials and methods

2.1. Materials

The Ti_3AlC_2 MAX phase was prepared as previously reported [66]. Lithium fluoride (LiF, 98%+) was purchased from Alfa Aesar. Hydrochloric acid (HCl, 37% [w/w], ACS reagent), dimethyl sulfoxide (DMSO, >99.5%), Acrylamide, *N,N′*-methylenebisacrylamide (MBAM), and potassium peroxide (KPS), were purchased from Sigma-Aldrich. All the chemicals were used without further treatment.

2.2. Instrumentation

Emulsions were made using a handheld emulsifier from BioSpec Products Inc. (model 985370). X-ray diffraction (XRD) was conducted on a Miniflex II (Rigaku) with a Cu-Kα radiation source ($\lambda = 1.5406$ Å). XPS was performed using an Omicron x-ray photoelectron spectrometer employing an Mg-sourced x-ray beam at 10 kV with aperture 3. SEM was performed on a JEOL JSM-7500F scanning electron microscope with the acceleration voltage of 5 kV and 20 kV for microscopy imaging and EDS imaging, respectively. Atomic force microscopy (AFM) was conducted on a Bruker Dimension Icon AFM. Computed tomography (CT) was performed on an x-ray microscopy (XRM, Zeiss, Inc. model Xradia 520 Versa) at 80 kV, 7 W. The 3D images of polyHIPE samples were obtained through software reconstruction. Thermogravimetric Analysis (TGA) was conducted on a TA instrument, TGA 5500, under nitrogen flow. The AC conductivity was obtained using a dielectric spectrometer; the samples were placed between two gold plates with a diameter of 1 cm. The volume percent of $Ti_3C_2T_x$ in the polyHIPEs was calculated based on the volume of Ti_3C_2 MXene ($V_{\mathrm{MXene}} = m/\rho_{\mathrm{MXene}}$, $\rho_{\mathrm{MXene}} = 3.7$ g cm^{-3} [67]) and the volume of polyHIPEs ($V_{\mathrm{polyHIPEs}} = \pi r^2 h$, where r is the radius of the polyHIPE cylinder and h is the thickness of the polyHIPE cylinder).

2.3. Preparation of $Ti_3C_2T_x$ nanosheets

$Ti_3C_2T_x$ nanosheets were obtained following our previously reported method. Briefly, 20 ml of 6 M aqueous HCl was prepared, and 1.6 g of LiF was added with continuous stirring. Then, 2 g of MAX powder was slowly added to this solution, and the mixture stirred continuously at 40 °C for 40 h. The resulting suspension was washed with deionized water and separated by centrifugation, with the supernatant discarded. The washing process of the pellet was repeated for several times until the supernatant reached pH ~6, as determined by litmus paper. The precipitate ($Ti_3C_2T_x$ clay) was then intercalated with DMSO at room temperature for 20 h with continuous stirring. Then, excess DMSO was removed by centrifugation followed by deionized water washing three times and centrifugation at 9000 rpm for 30 min, discarding supernatant, then adding fresh water and bath sonication for 1 h. The $Ti_3C_2T_x$ nanosheets were obtained by centrifuging the suspension at 3500 rpm for 45 min and collecting the supernatant. The concentration of as-prepared $Ti_3C_2T_x$ nanosheet solutions was determined to be 8 mg ml^{-1} by preparing a buckypaper by vacuum-assisted filtration, using a known volume of solution, then determining the mass of the buckypaper and back calculating concentration.

3. Preparation of $Ti_3C_2T_x$ polyHIPEs

PolyHIPEs were prepared by polymerizing the continuous phase of the HIPEs. To form HIPEs, we used NaCl to flocculate $Ti_3C_2T_x$ nanosheets and then used the NaCl-flocculated $Ti_3C_2T_x$ nanosheets to stabilize oil-in-water Pickering HIPEs [65]. A typical dodecane-in-water Pickering HIPE stabilized by 2 mg ml^{-1} $Ti_3C_2T_x$ was prepared as follows. First, an aqueous solution of 400 mg of acrylamide, 10 mg of MBAM, 10 mg of KPS, and 0.025 M NaCl was prepared in 1.5 ml water. Then a 0.5 ml of $Ti_3C_2T_x$ nanosheets (8 mg ml^{-1}) was added to the solution to make a 2 mg ml^{-1} dispersion with a total volume of 2 ml. Then, 6 ml of dodecane was added to the aqueous solution. The mixture was agitated using a hand-held emulsifier for 1 min (20 s on, 5 s off for three cycles), and the dark and viscous HIPEs are formed. To prepare the polyHIPEs, the HIPEs were heated at 70 °C on an aluminum heating block for 1 min to initiate the polymerization, and then the vial was left without stirring at room temperature for 24 h. The hydrogels were then immersed in the ethanol for 30 min and repeated five times to remove the dodecane and the absorbed water. The polyHIPEs were obtained by drying under reduced pressure for 24 h. The content of $Ti_3C_2T_x$ in the polyHIPEs was obtained by dividing the mass of $Ti_3C_2T_x$ added to the solution by the total mass of the dried polyHIPE sample. For example, the weight percent of $Ti_3C_2T_x$ was 1.1 wt%, 1.5 wt%, 2.1 wt%, and 2.5 wt% for the 2 mg ml^{-1}, 3 mg ml^{-1}, 4 mg ml^{-1}, and 5 mg ml^{-1} polyHIPE samples, respectively.

4. Results and discussion

4.1. Preparation and characterization of $Ti_3C_2T_x$ nanosheets

$Ti_3C_2T_x$ nanosheets, the most commonly used and widely available MXene, were used in this work. The nanosheets were synthesized and characterized, as previously reported [68]. First, an aqueous solution of LiF/HCl was used to selectively etch the Al layer from Ti_3AlC_2 MAX powder and then $Ti_3C_2T_x$ clay was obtained after washing with water to remove excess acid. A transparent and dark green aqueous dispersion of $Ti_3C_2T_x$ nanosheets was obtained by intercalation of the clay with DMSO and exfoliation. Figure 1(a) shows the XRD curve of a free-standing $Ti_3C_2T_x$ film obtained by vacuum-assisted filtration of the aqueous nanosheet dispersion. A characteristic 002 peak around 6.8° is observed, indicating successful etching and exfoliation of $Ti_3C_2T_x$ nanosheets. The AFM image of drop-cast $Ti_3C_2T_x$ nanosheets shows single layer nanosheets with lateral sizes ranging from hundreds of nanometers to a few micrometers and a thickness of around 1.5 nm (figures 1(b) and S1). Freeze-dried $Ti_3C_2T_x$ nanosheets were characterized by SEM (figure S2), which also shows individual nanosheets, indicating their successful formation. Further, the chemical composition of a free-standing $Ti_3C_2T_x$ film was characterized by XPS (figures 1(c), (d) and S3). The survey XPS spectrum (figure 1(c)) confirms the presence of C, O, Ti, F elements, and deconvolution of the high-resolution Ti 2p spectrum (figure 1(d)) into Ti-C, Ti^{2+}, Ti^{3+}, TiO_2, Ti-F, shows only 2.5 at% of TiO_2 (binding energy of 458.7 eV, table S1); this indicates that little oxidation (i.e. formation of TiO_2) occurred during etching, intercalation, or exfoliation.

4.2. Formation of $Ti_3C_2T_x$ polyHIPEs

To prepare $Ti_3C_2T_x$ polyHIPEs, dodecane-in-water HIPEs were first formed using NaCl-flocculated $Ti_3C_2T_x$ nanosheets as the 2D particle stabilizers, followed by polymerization of the water-soluble monomer and drying of the sample. As shown in figure 2(a), 75 vol% of dodecane was added into an aqueous solution that contained NaCl flocculated $Ti_3C_2T_x$ nanosheets, acrylamide (monomer), *N,N′*-MBAM (crosslinker), and KPS (radical initiator). The mixture was agitated to form dodecane-in-water HIPEs, which were dark, viscous, and gel-like solutions. The HIPE was then heated at 70 °C for 1 min to initiate polymerization, then allowed to sit at room temperature for 24 h (figure 2(a, ii)). Polymerization and crosslinking of acrylamide in the continuous aqueous phase (e.g. formation of polyacrylamide (PAAm)) were expected to form a water-swollen polymer around the oil droplets, such that drying would yield a highly porous morphology. After polymerization, the polyHIPE sample was washed with ethanol to remove both the oil droplets from within the structure and also the water that was swelling the polymer, then the sample was dried under reduced pressure. $Ti_3C_2T_x$-polymer polyHIPEs were obtained as a single dark grey material (figure 2(a, iii)). The morphology was confirmed by the SEM images of $Ti_3C_2T_x$ polyHIPEs; figures 2(b)–(e) are cross-sectional SEM images of the polyHIPEs formed from different concentrations of nanosheets, highlighting the porous structure with interconnected pores. Due to shrinkage during polymerization and/or the drying process, small holes (termed windows) form between adjacent droplets. High-resolution SEM images (figure S4) show a flaky, rough surface inside the pores, suggesting the presence of $Ti_3C_2T_x$ nanosheets. In contrast, smooth surfaces were observed on the surface of the fractured polymer structure, as is shown in figure S4(a). We note that the pores of the $Ti_3C_2T_x$-PAAm polyHIPEs are coated with $Ti_3C_2T_x$ nanosheets and that these pores were created by removal of oil droplets; this is in contrast to the more common $Ti_3C_2T_x$-containing polymer hydrogels where nanosheets are incorporated within the polymer networks and contained by polymer chain entanglements, ionic interactions, and hydrogen and/or covalent bonding [69, 70].

Changing the $Ti_3C_2T_x$ concentration led to varied pore morphology of the resulting $Ti_3C_2T_x$ polyHIPEs. Four different $Ti_3C_2T_x$ concentrations (2 mg ml^{-1}, 3 mg ml^{-1}, 4 mg ml^{-1}, and 5 mg ml^{-1})

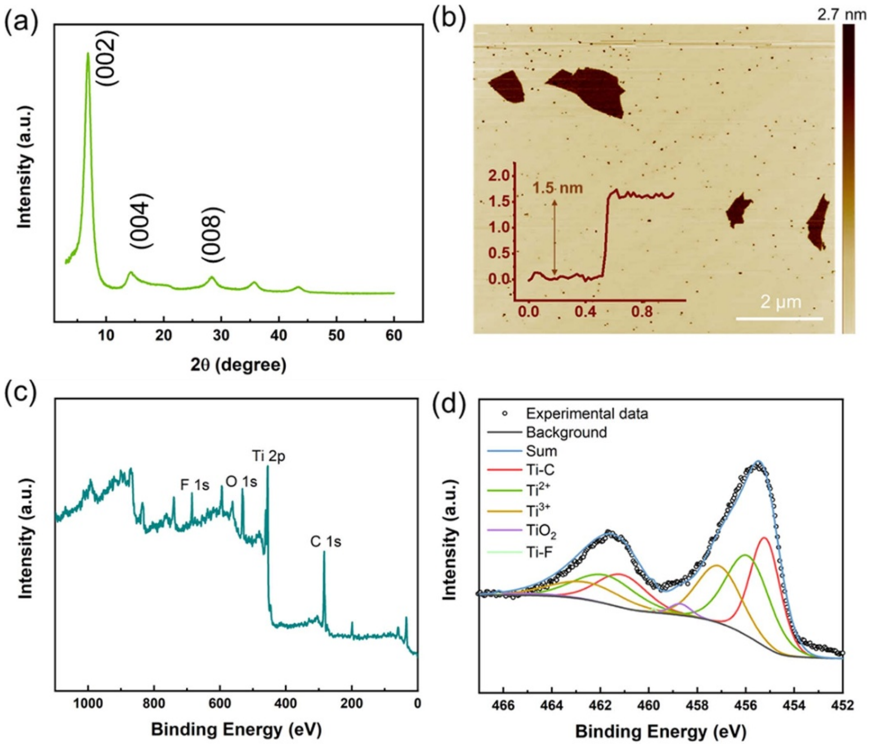

Figure 1. Characterization of $Ti_3C_2T_x$ nanosheets, (a) XRD spectrum of the vacuum-assisted filtered film, (b) AFM image of drop-cast dispersion (inset shows height profile of the $Ti_3C_2T_x$ nanosheet denoted by the white line), (c) XPS survey spectrum of vacuum-assisted filtered film, (d) high resolution and deconvoluted Ti 2p XPS spectrum of vacuum-assisted filtered film.

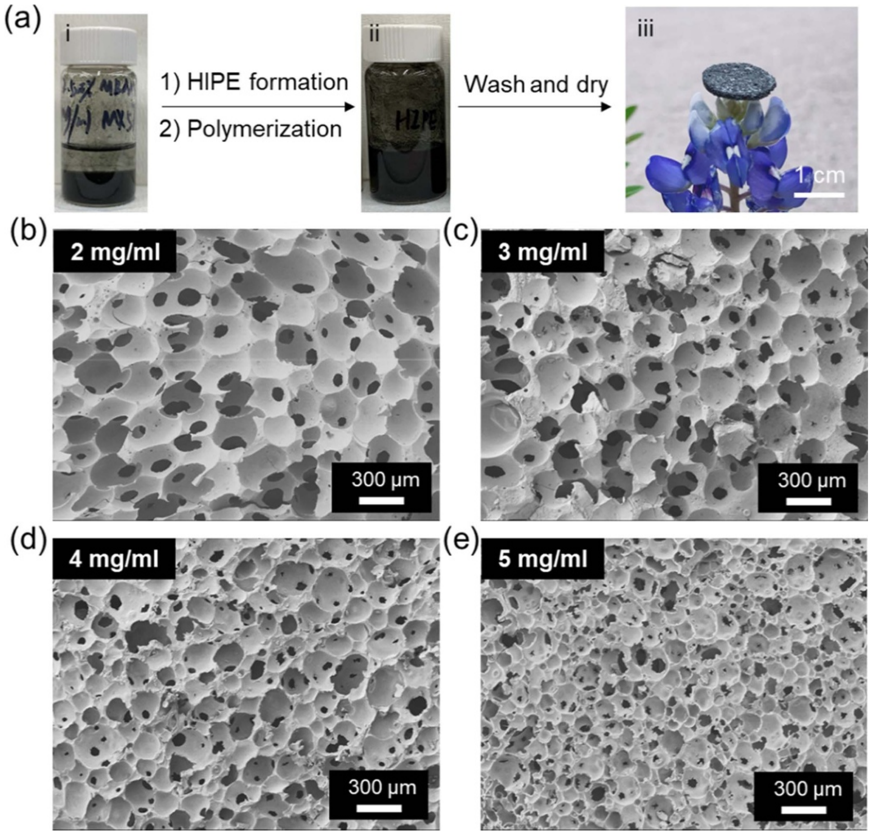

Figure 2. Formation and characterization of $Ti_3C_2T_x$ polyHIPEs, (a) digital images of (i) vial before HIPE formation, (ii) vial containing polyHIPEs, and (iii) porous macroscopic structure upon a Texas bluebonnet flower ($Ti_3C_2T_x$ concentration 2 mg ml^{-1}), (b)–(e) SEM images of $Ti_3C_2T_x$ polyHIPEs prepared with different $Ti_3C_2T_x$ concentrations ((b) 2 mg ml^{-1}, (c) 3 mg ml^{-1}, (d) 4 mg ml^{-1}, (e) 5 mg ml^{-1}).

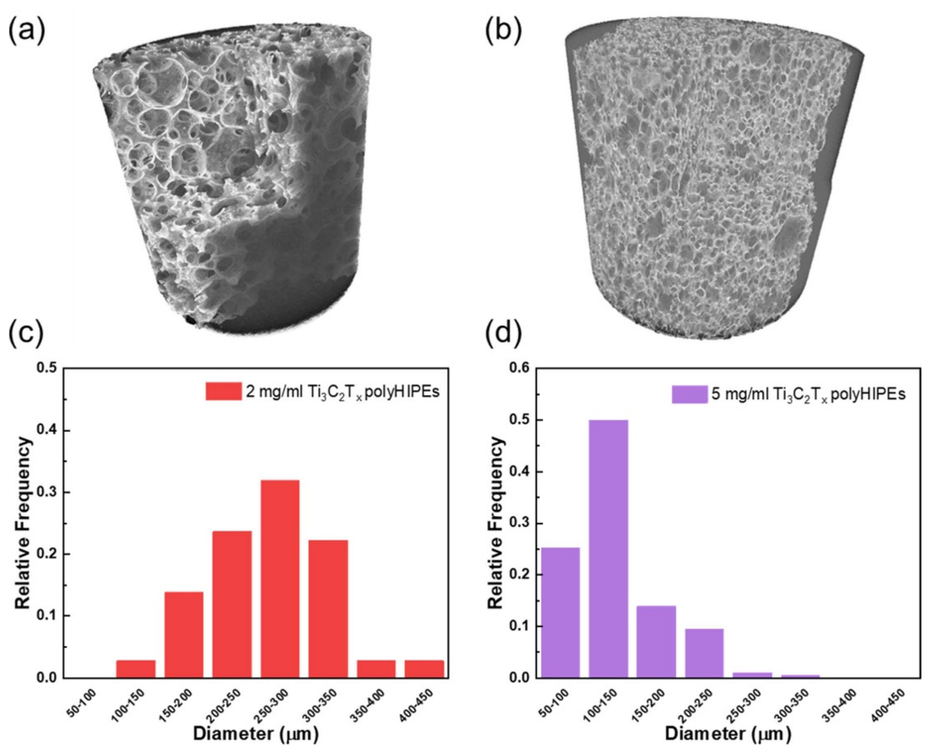

Figure 3. Computed tomography (CT) scan of $Ti_3C_2T_x$ polyHIPEs with, (a) $Ti_3C_2T_x$ concentrations of 2 mg ml^{-1}, and (b) 5 mg ml^{-1}; the diameter of these two samples is 2.5 mm. The histogram of pore size distribution of $Ti_3C_2T_x$ polyHIPEs determined using Image J analysis on the SEM images corresponding to (c) 2 mg ml^{-1} (with an average of 264.3 μm and standard deviation of 61.8 μm), and (d) 5 mg ml^{-1} (with an average of 130.7 μm and standard deviation of 45.5 μm).

were used to stabilize the dodecane-in-water HIPEs, with higher concentrations expected to give smaller oil droplets and thus smaller pores in the polyHIPEs [71, 72]. This is because higher surfactant concentration ($Ti_3C_2T_x$ nanosheets in this case) give more available surface area of surfactant, leading to the formation of smaller emulsion droplets at the same oil/water ratio. Upon polymerization, no substantial change in droplet size is expected and thus HIPEs with higher nanosheet loading are expected to give smaller pores. As expected, we observed smaller pores in the $Ti_3C_2T_x$ polyHIPEs prepared with higher $Ti_3C_2T_x$ concentrations. As shown in figures 2(b)–(e), the pore size consistently decreases with the increase of $Ti_3C_2T_x$ concentration from 2 mg ml^{-1} to 5 mg ml^{-1}. Differences in the pore size distribution are quantified by Image J analysis [21, 64]: pore size decreases from 200–350 μm for the 2 mg ml^{-1} sample (>80%, with an average of 264.3 μm), to 50–150 μm for the 5 mg ml^{-1} sample (>80%, with an average of 130.7 μm) (figures 3(c), (d) and S5). This is also supported by the 3D construct of $Ti_3C_2T_x$ polyHIPE samples obtained by CT. In both the 2 mg ml^{-1} and 5 mg ml^{-1}, samples, highly porous polyHIPE structures were observed (figures 3(a) and (b)), with significantly smaller pores in the 5 mg ml^{-1} sample compared to 2 mg ml^{-1} sample. This confirms the ability to tune the pore size in the $Ti_3C_2T_x$ polyHIPEs by modifying the concentration of $Ti_3C_2T_x$ nanosheets used.

To confirm the structure of $Ti_3C_2T_x$ polyHIPEs as porous PAAm with pores coated with $Ti_3C_2T_x$, EDS and XPS were used. Figure 4(a) shows the SEM image of 2 mg ml^{-1} $Ti_3C_2T_x$ polyHIPEs and the corresponding carbon and titanium mapping. The mapping clearly shows that the fractured polymer backbone is rich in carbon (bright red) and the surface of the pore is rich in titanium (bright blue). In addition, the dark red regions (middle image, figure 4(a)) show the uniform distribution of carbon on the surface of the pores, supporting the presence of $Ti_3C_2T_x$ nanosheets. Similarly, the EDS mapping images of polyHIPEs from higher $Ti_3C_2T_x$ concentration (3 mg ml^{-1}, 4 mg ml^{-1}, and 5 mg ml^{-1}) show the polymer structure is rich in carbon and the surface of the pores are rich in titanium (figure S6), consistent with a porous polymer structure coated with $Ti_3C_2T_x$ nanosheets. XPS, a surface-sensitive technique, was also used to analyze the elemental compositions of the polyHIPEs. The survey spectrum shows the presence of C, O, N, and Ti elements in the 2 mg ml^{-1} $Ti_3C_2T_x$ polyHIPEs (figure 4(b)), with the presence of nitrogen due to –NH_2 in the PAAm (figure S7(a)). This was also verified by the deconvoluted high-resolution C 1s and O 1s spectrum (figures S7(b) and (c), which showed the presence of C–N, O=C–N bonding in the polyHIPEs. The high-resolution Ti 2p spectrum is deconvoluted into Ti-C, Ti^{2+}, Ti^{3+}, TiO_2, and Ti-F binding energies (figure 4(c)). Notably, the TiO_2 peak (purple, binding energy at 458.7 eV, table S2)

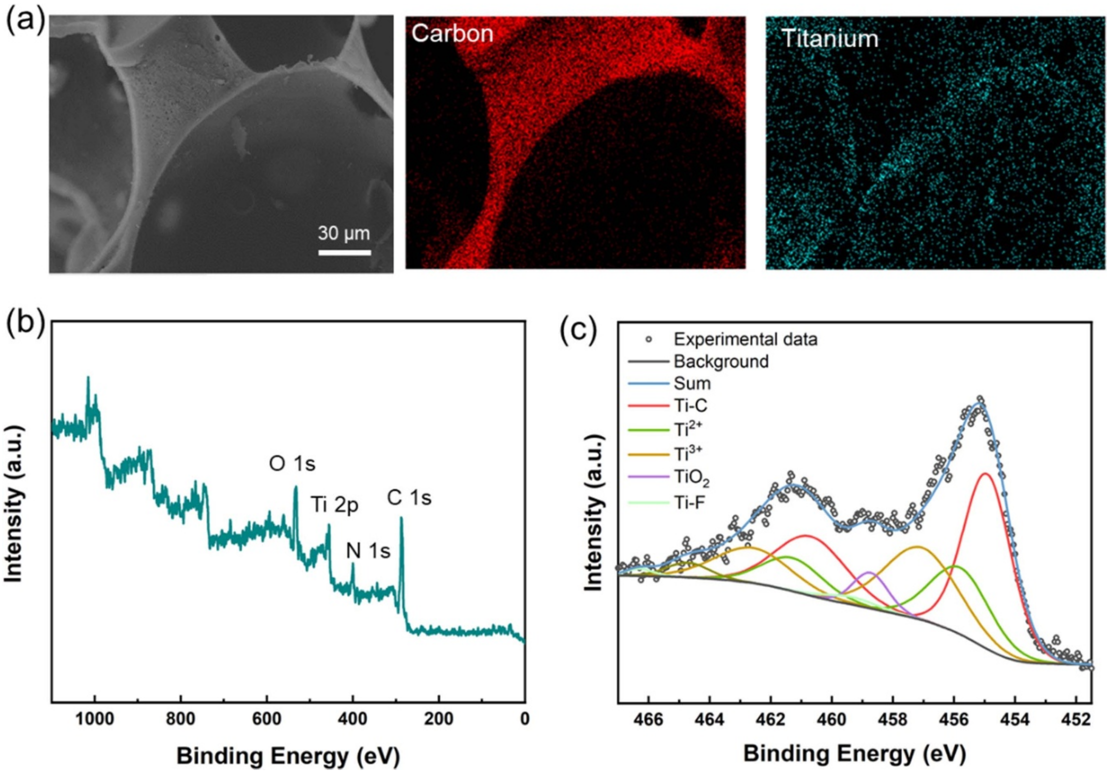

Figure 4. Characterization of the chemical composition of $Ti_3C_2T_x$ polyHIPEs prepared from 2 mg ml^{-1} concentration of nanosheets, (a) SEM and EDS mapping (red = carbon, blue = titanium), (b) XPS survey spectrum, (c) high resolution Ti 2p spectrum.

is small compared to those of Ti-C, Ti^{2+}, and Ti^{3+} and only contributes around 6 at% of the Ti 2p signal. Since the as-prepared $Ti_3C_2T_x$ nanosheets contained 2.5 at% of TiO_2, some oxidation of the titanium in the nanosheets does occur during the formation of the polyHIPEs, which may be attributed to oxidation by KPS during polymerization. Survey, high-resolution Ti 2p, C 1s, O 1s, and N 1s XPS spectra (figures S8–S10) were collected for the other $Ti_3C_2T_x$ polyHIPE samples ($Ti_3C_2T_x$ concentration: 3 mg ml^{-1}, 4 mg ml^{-1}, and 5 mg ml^{-1}), all confirming the presence of C, O, N, and Ti elements. The TiO_2 content has a decreased contribution with increasing concentration of $Ti_3C_2T_x$: 3 mg ml^{-1}, 4 mg ml^{-1}, and 5 mg ml^{-1} $Ti_3C_2T_x$ polyHIPE samples have TiO_2 content of 4.5 at%, 4.1 at%, and 3.6 at% (binding energy at 458.7 eV, 458.8 eV, and 458.8 eV, tables S3–S5), respectively. We attribute this trend to the fact that at higher concentrations of $Ti_3C_2T_x$ nanosheets, close and dense nanosheet aggregates form, and the nanosheets are sterically protected from oxidation. This is consistent with literature reports that higher concentrations of MXene slow oxidation [67]. Notably, maintaining $Ti_3C_2T_x$ composition, i.e. preventing oxidation, is crucial to maintaining the unique properties of the nanosheets [73, 74].

The thermal stability of $Ti_3C_2T_x$ polyHIPE samples were characterized by TGA. Figure S11 shows the weight loss profiles of polyHIPE samples with different $Ti_3C_2T_x$ concentrations. For comparison, a pure cross-linked PAAm sample was characterized and showed two distinct weight loss steps, one at 269 °C (∼25 wt%) and the second at 371 °C (∼50 wt%), in agreement with prior reports [75, 76]. Similar weight loss profiles were observed for all $Ti_3C_2T_x$ polyHIPE samples (2 mg ml^{-1}, 3 mg ml^{-1}, 4 mg ml^{-1}, 5 mg ml^{-1}) as for the pure cross-linked polymer (figures S11(b)–(e)). For example, two steps of weight loss were observed at 260 °C (∼26 wt%) and 375 °C (∼47 wt%) in the 2 mg ml^{-1} $Ti_3C_2T_x$ polyHIPE sample. This confirms the successful formation of cross-linked PAAm in the polyHIPE samples and indicates that the presence of $Ti_3C_2T_x$ nanosheets has little impact on the thermal stability of PAAm.

4.3. Electrical properties of $Ti_3C_2T_x$ polyHIPEs

Given the organization of the $Ti_3C_2T_x$ nanosheets in the polyHIPEs and lack of titanium oxidation, the porous polyHIPEs are expected to be electrically conductive, even though PAAm itself is insulating. The AC conductivities of polyHIPE samples with different $Ti_3C_2T_x$ concentrations were measured using a dielectric spectrometer (figure 5(a)). Over the frequency ranging from 0.3 Hz to 10 MHz, an increase in AC conductivity is observed with increase of $Ti_3C_2T_x$ concentration. For example, the AC conductivity is increased from 4×10^{-9} S cm^{-1} for 2 mg ml^{-1}

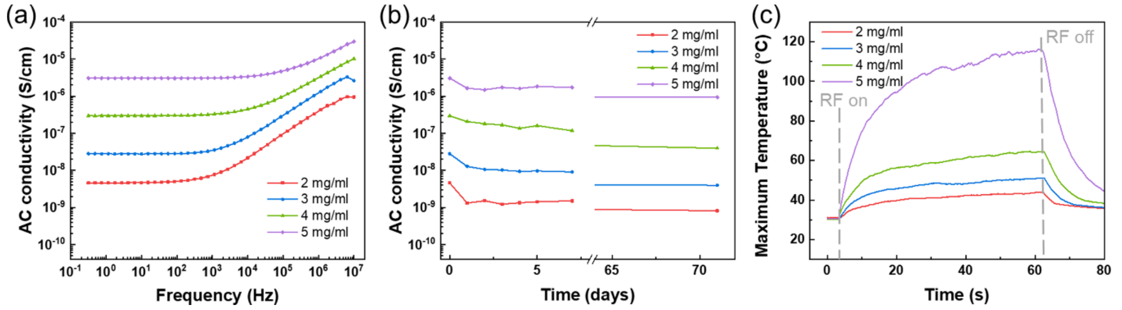

Figure 5. (a) AC conductivity of $Ti_3C_2T_x$ polyHIPEs with different $Ti_3C_2T_x$ concentrations, (b) AC conductivity of different $Ti_3C_2T_x$ polyHIPEs at low frequency (0.3 Hz) as a function of storage time under ambient conditions, (c) RF heating of $Ti_3C_2T_x$ polyHIPEs at 125 MHz at 1 W.

$Ti_3C_2T_x$ polyHIPEs to 3×10^{-6} S cm^{-1} for 5 mg ml^{-1} $Ti_3C_2T_x$ polyHIPEs at low frequency (0.3 Hz); at high frequency (10 MHz), the AC conductivity is increased from 1×10^{-6} S cm^{-1} for 2 mg ml^{-1} $Ti_3C_2T_x$ polyHIPEs to 3×10^{-5} S cm^{-1} for 5 mg ml^{-1} $Ti_3C_2T_x$ polyHIPEs. The volume percent of $Ti_3C_2T_x$ in polyHIPEs are 0.065%, 0.073%, 0.080%, and 0.088% for samples for the 2 mg ml^{-1}, 3 mg ml^{-1}, 4 mg ml^{-1}, and 5 mg ml^{-1} samples, respectively. The volume percent of $Ti_3C_2T_x$ nanosheets in polyHIPEs to form a percolated network is significantly lower than for bulk MXene composite film (e.g. 1.7 vol% in $Ti_3C_2T_x$/PAAm composite film [77], or 0.9 vol% in $Ti_3C_2T_x$/natural rubber composite film [78]). Figure 5(b) shows the AC conductivity for the $Ti_3C_2T_x$ polyHIPEs at low frequency (0.3 Hz) as a function of storage time in an open atmosphere. Whereas a decrease of AC conductivity is observed for all polyHIPEs over the first three days, only a slight decrease in conductivity is observed from day 3 to day 70. For example, for the 2 mg ml^{-1} $Ti_3C_2T_x$ polyHIPEs, conductivity decreased from 4×10^{-9} S cm^{-1} to 1×10^{-9} S cm^{-1} at day 3, and 8×10^{-10} S cm^{-1} at day 71. At high frequency (10 MHz), the AC conductivity shows little decrease for all four samples, as is shown in figure S12. For example, for the 5 mg ml^{-1} $Ti_3C_2T_x$ polyHIPEs, the AC conductivity decreased from 3×10^{-5} S cm^{-1} to 2×10^{-5} S cm^{-1} at day 71. The slow oxidation indicates the nanosheets are protected by the polymer matrix and not exposed to water [79].

In addition to AC conductivity, RF heating was performed on the $Ti_3C_2T_x$ polyHIPEs, as is shown in figure 5(c). One RF heating cycle was demonstrated for the four different $Ti_3C_2T_x$ polyHIPE samples at 125 MHz at 1 W. In only a few seconds, rapid heating was observed for all samples in response to low power RF due to the presence of the nanosheets [80]. For example, an increase in temperature from 30 to 38 °C was observed in response to the application of RF for 10 s in the 2 mg ml^{-1} $Ti_3C_2T_x$ polyHIPEs. Furthermore, higher concentration $Ti_3C_2T_x$ polyHIPEs show much rapid RF heating at the same conditions: the 5 mg ml^{-1} $Ti_3C_2T_x$ polyHIPE sample exhibits the highest RF heating response at 1 W (from 30 °C to 85 °C in 10 s). This can be attributed to the higher electrical conductivity of the 5 mg ml^{-1} $Ti_3C_2T_x$ polyHIPEs compared to the other three samples, resulting in the highest response to the RF field. These data indicate the formation of a percolated conductive network in the polyHIPEs.

5. Conclusion

Electrically conductive $Ti_3C_2T_x$-polymer polyHIPEs were synthesized via polymerization of the continuous phase of oil-in-water HIPEs which were stabilized by salt flocculated $Ti_3C_2T_x$ nanosheets. Polymerization of acrylamide and crosslinker in the continuous aqueous phase led to the formation of a polyHIPE with pores lined with $Ti_3C_2T_x$ nanosheets and filled with oil; after solvent removal and drying, a porous monolithic structure was produced, with the size of the pores controlled by the $Ti_3C_2T_x$ nanosheet concentration. For polyHIPEs prepared from different concentrations of $Ti_3C_2T_x$, the composition and morphology were verified by SEM, EDS, and XPS. The porous structure with pores lined with $Ti_3C_2T_x$ were electrically conductive, giving an AC conductivity of 10^{-6} S cm^{-1} at low frequency with 5 mg ml^{-1} of $Ti_3C_2T_x$. Further, the $Ti_3C_2T_x$ nanosheets within the polyHIPEs are stable to oxidation over months, showing a limited decrease in electrical conductivity upon storage under ambient conditions. This work presents a simple and scalable approach to accessing porous MXene-polymer composites with tailorable pore morphology and good oxidation stability of the nanosheets, with potential applications in electronics and catalysis. This approach avoids the use of organic small molecule co-surfactants, simplifying and expanding the use of MXene/polymer composites for diverse applications. Future work can address the impact of MXene nanosheet terminal groups both on emulsion formation and polyHIPE synthesis, as well as their use to tune chemical interactions during polymerization.

Data availability statement

The data generated and/or analysed during the current study are not publicly available for legal/ethical reasons but are available from the corresponding author on reasonable request.

Acknowledgments

The authors thank Texas A&M University for financial support. EP thanks NSF DMR Award #2103183. We would like to thank TAMU Materials Characterization Facilities for the use of XPS, AFM, SEM, and EDS. Use of the Texas A&M University Soft Matter Facility for TGA is acknowledged. We also thank Dr Mustafa Akbulut's group and graduate student Shuhao Liu at Texas A&M University for the help in the use of the Zetasizer instrument. We acknowledge the help from Xiaofei Zhao in MXene synthesis. We also acknowledge the help from Dr Mohammed Saed for the measurement of S-parameters using VNA instruments. We acknowledge the help from Ian Echols for the analysis of AFM images.

Conflict of interest

The authors declare no conflicts of interest.

Author contributions

The manuscript was written through contributions of all authors. Huaixuan Cao carried out laboratory experiments and data analysis on sample preparation (MXene synthesis, polyHIPE formation) and characterization, wrote draft of manuscript; Yifei Wang assisted with laboratory experiments and characterization on thermal properties of polyHIPEs; Anubhav Sarmah and Kailash Dhondiram Arole assisted with laboratory experiments and data analysis on thermal conductivity and RF heating applications. Kai-Wei Liu assisted with CT scanning and data analysis. Zeyi, Tan assisted with the synthesis of MXene. Jodie L Lutkenhaus and Miladin Radovic revised manuscript and provided critical feedback. Emily B Pentzer and Micah J Green supervised the project. All authors discussed the results and contributed to the final manuscript. All authors have given approval to the final version of the manuscript.

ORCID iDs

Huaixuan Cao https://orcid.org/0000-0003-0848-0339
Yifei Wang https://orcid.org/0000-0003-0110-8147
Zeyi Tan https://orcid.org/0000-0002-0536-6365
Kailash Dhondiram Arole https://orcid.org/0000-0002-4516-889X
Jodie L Lutkenhaus https://orcid.org/0000-0002-2613-6016
Miladin Radovic https://orcid.org/0000-0003-4571-2848
Micah J Green https://orcid.org/0000-0001-5691-0861
Emily B Pentzer https://orcid.org/0000-0001-6187-6135

References

[1] Silverstein M S 2014 Emulsion-templated porous polymers: a retrospective perspective *Polymer* **55** 304–20

[2] Zhang H and Cooper A I 2005 Synthesis and applications of emulsion-templated porous materials *Soft Matter* **1** 107–13

[3] Pulko I and Krajnc P 2012 High internal phase emulsion templating—a path to hierarchically porous functional polymers *Macromol. Rapid Commun.* **33** 1731–46

[4] Silverstein M S and Cameron N R 2010 PolyHIPEs—porous polymers from high internal phase emulsions *Encyclopedia of Polymer Science and Technology* (New York: Wiley) (https://doi.org/10.1002/0471440264.pst571)

[5] Gurevitch I and Silverstein M S 2010 Polymerized pickering HIPEs: effects of synthesis parameters on porous structure *J. Polym. Sci.* A **48** 1516–25

[6] Foudazi R 2021 HIPEs to polyHIPEs *React. Funct. Polym.* **164** 104917

[7] Wang Q, Liu Y, Chen J, Du Z and Mi J 2016 Control of uniform and interconnected macroporous structure in polyHIPE for enhanced CO_2 adsorption/desorption kinetics *Environ. Sci. Technol.* **50** 7879–88

[8] Zowada R and Foudazi R 2019 Porous hydrogels embedded with hydrated ferric oxide nanoparticles for arsenate removal *ACS Appl. Polym. Mater.* **1** 1006–14

[9] Kadhim M, Oila A and Bull S J 2019 PolyHIPEs for water treatment *J. Phys.: Conf. Ser.* **1294** 052072

[10] Huang Y, Ruan G, Ruan Y, Zhang W, Li X, Du F, Hu C and Li J 2018 Hypercrosslinked porous polymers hybridized with graphene oxide for water treatment: dye adsorption and degradation *RSC Adv.* **8** 13417–22

[11] Mrówka J, Gackowski M, Lityńska-Dobrzyńska L, Bernasik A, Kosydar R, Drelinkiewicz A and Hasik M 2020 Poly(methylvinylsiloxane)-based high internal phase emulsion-templated materials (polyHIPEs)—preparation, incorporation of palladium, and catalytic properties *Ind. Eng. Chem. Res.* **59** 19485–99

[12] Yang L, Jiang C, Yan J, Shen Y, Chen Y, Xu L and Zhu H 2020 Structuring the reduced graphene oxide/polyHIPE foam for piezoresistive sensing via emulsion-templated polymerization *Composites* A **134** 105898

[13] Yang L, Liu Y, Filipe C D M, Ljubic D, Luo Y, Zhu H, Yan J and Zhu S 2019 Development of a highly sensitive, broad-range hierarchically structured reduced graphene oxide/polyHIPE foam for pressure sensing *ACS Appl. Mater. Interfaces* **11** 4318–27

[14] Martín C, Merino S, González-Domínguez J M, Rauti R, Ballerini L, Prato M and Vázquez E 2017 Graphene improves the biocompatibility of polyacrylamide hydrogels: 3D polymeric scaffolds for neuronal growth *Sci. Rep.* **7** 10942

[15] Zhang H and Cooper A I 2002 Synthesis of monodisperse emulsion-templated polymer beads by oil-in-water-in-oil (O/W/O) sedimentation polymerization *Chem. Mater.* **14** 4017–20

[16] Zhang S and Chen J 2007 Synthesis of open porous emulsion-templated monoliths using cetyltrimethylammonium bromide *Polymer* **48** 3021–5

[17] Li Z, Ming T, Wang J and Ngai T 2009 High internal phase emulsions stabilized solely by microgel particles *Angew. Chem., Int. Ed.* **48** 8490–3

[18] Ikem V O, Menner A and Bismarck A 2009 High internal phase emulsions stabilized solely by functionalized silica particles *Angew. Chem., Int. Ed.* **48** 632

[19] Claire Hermant M, Klumperman B and Koning C E 2009 Conductive pickering-poly(high internal phase emulsion) composite foams prepared with low loadings of single-walled carbon nanotubes *Chem. Commun.* 2738–40

[20] Hermant M C, Verhulst M, Kyrylyuk A V, Klumperman B and Koning C E 2009 The incorporation of single-walled carbon nanotubes into polymerized high internal phase emulsions to create conductive foams with a low percolation threshold *Compos. Sci. Technol.* **69** 656–62

[21] Yi W, Wu H, Wang H and Du Q 2016 Interconnectivity of macroporous hydrogels prepared via graphene oxide-stabilized pickering high internal phase emulsions *Langmuir* **32** 982–90

[22] Zheng Z, Zheng X, Wang H and Du Q 2013 Macroporous graphene oxide–polymer composite prepared through pickering high internal phase emulsions *ACS Appl. Mater. Interfaces* **5** 7974–82

[23] Huang Y, Zhang W, Ruan G, Li X, Cong Y, Du F and Li J 2018 Reduced graphene oxide-hybridized polymeric high-internal phase emulsions for highly efficient removal of polycyclic aromatic hydrocarbons from water matrix *Langmuir* **34** 3661–8

[24] Wong L L C, Barg S, Menner A, Do Vale Pereira P, Eda G, Chowalla M, Saiz E and Bismarck A 2014 Macroporous polymer nanocomposites synthesised from high internal phase emulsion templates stabilised by reduced graphene oxide *Polymer* **55** 395–402

[25] Gulati A and Kakkar R 2020 Graphene-based adsorbents for water remediation by removal of organic pollutants: theoretical and experimental insights *Chem. Eng. Res. Des.* **153** 21–36

[26] Cheng C, Liu Z, Li X, Su B, Zhou T and Zhao C 2014 Graphene oxide interpenetrated polymeric composite hydrogels as highly effective adsorbents for water treatment *RSC Adv.* **4** 42346–57

[27] Woltornist S J, Carrillo J-M Y, Xu T O, Dobrynin A V and Adamson D H 2015 Polymer/pristine graphene based composites: from emulsions to strong, electrically conducting foams *Macromolecules* **48** 687–93

[28] Naguib M, Kurtoglu M, Presser V, Lu J, Niu J, Heon M, Hultman L, Gogotsi Y and Barsoum M W 2011 Two-dimensional nanocrystals produced by exfoliation of Ti_3AlC_2 *Adv. Mater.* **23** 4248–53

[29] Ghidiu M, Lukatskaya M R, Zhao M-Q, Gogotsi Y and Barsoum M W 2014 Conductive two-dimensional titanium carbide ‘clay’ with high volumetric capacitance *Nature* **516** 78–81

[30] Naguib M, Mochalin V N, Barsoum M W and Gogotsi Y 2014 25th anniversary article: MXenes: a new family of two-dimensional materials *Adv. Mater.* **26** 992–1005

[31] Anasori B, Lukatskaya M R and Gogotsi Y 2017 2D metal carbides and nitrides (MXenes) for energy storage *Nat. Rev. Mater.* **2** 16098

[32] Lukatskaya M R *et al* 2017 Ultra-high-rate pseudocapacitive energy storage in two-dimensional transition metal carbides *Nat. Energy* **2** 17105

[33] Orangi J, Hamade F, Davis V A and Beidaghi M 2020 3D printing of additive-free 2D $Ti_3C_2T_x$ (MXene) ink for fabrication of micro-supercapacitors with ultra-high energy densities *ACS Nano* **14** 640–50

[34] Yun J, Natu V, Echols I, Thakur R M, Cao H, Tan Z, Radovic M, Green M J, Barsoum M W and Lutkenhaus J L 2022 Anion identity and time scale affect the cation insertion energy storage mechanism in $Ti_3C_2T_x$ MXene multilayers *ACS Energy Lett.* **7** 1828–34

[35] Sarang K, Zhao X, Holta D, Cao H, Arole K, Flouda P, Oh E-S, Radovic M, Green M J and Lutkenhaus J L 2021 Carbon additive-free crumpled $Ti_3C_2T_X$ MXene-encapsulated silicon nanoparticle anodes for lithium-ion batteries *ACS Appl. Energy Mater.* **4** 10762–73

[36] Saha S, Arole K, Radovic M, Lutkenhaus J L and Green M J 2021 One-step hydrothermal synthesis of porous $Ti_3C_2T_z$ MXene/rGO gels for supercapacitor applications *Nanoscale* **13** 16543–53

[37] Gao G, O’Mullane A P and Du A 2017 2D MXenes: a new family of promising catalysts for the hydrogen evolution reaction *ACS Catal.* **7** 494–500

[38] Morales-García Á, Calle-Vallejo F and Illas F 2020 MXenes: new horizons in catalysis *ACS Catal.* **10** 13487–503

[39] Johnson D, Lai H-E, Hansen K, Balbuena P B and Djire A 2022 Hydrogen evolution reaction mechanism on Ti_3C_2 MXene revealed by in situ/operando Raman spectroelectrochemistry *Nanoscale* **14** 5068–78

[40] Pei Y, Zhang X, Hui Z, Zhou J, Huang X, Sun G and Huang W 2021 $Ti_3C_2T_X$ MXene for sensing applications: recent progress, design principles, and future perspectives *ACS Nano* **15** 3996–4017

[41] Shahzad F, Alhabeb M, Hatter C B, Anasori B, Man Hong S, Koo C M and Gogotsi Y 2016 Electromagnetic interference shielding with 2D transition metal carbides (MXenes) *Science* **353** 1137

[42] Song P, Liu B, Qiu H, Shi X, Cao D and Gu J 2021 MXenes for polymer matrix electromagnetic interference shielding composites: a review *Compos. Commun.* **24** 100653

[43] Iqbal A, Kwon J, Kim M K and Koo C M 2021 MXenes for electromagnetic interference shielding: experimental and theoretical perspectives *Mater. Today Adv.* **9** 100124

[44] Sun R, Zhang H-B, Liu J, Xie X, Yang R, Li Y, Hong S and Yu Z-Z 2017 Highly conductive transition metal carbide/carbonitride(MXene)@polystyrene nanocomposites fabricated by electrostatic assembly for highly efficient electromagnetic interference shielding *Adv. Funct. Mater.* **27** 1702807

[45] Cao H *et al* 2021 Synthesis and electronic applications of particle-templated $Ti_3C_2T_z$ MXene–polymer films via pickering emulsion polymerization *ACS Appl. Mater. Interfaces* **13** 51556–66

[46] Han M, Shuck C E, Rakhmanov R, Parchment D, Anasori B, Koo C M, Friedman G and Gogotsi Y 2020 Beyond $Ti_3C_2T_x$: MXenes for electromagnetic interference shielding *ACS Nano* **14** 5008–16

[47] Zhao S, Zhang H-B, Luo J-Q, Wang Q-W, Xu B, Hong S and Yu Z-Z 2018 Highly electrically conductive three-dimensional $Ti_3C_2T_x$ MXene/reduced graphene oxide hybrid aerogels with excellent electromagnetic interference shielding performances *ACS Nano* **12** 11193–202

[48] Li X, Yin X, Xu H, Han M, Li M, Liang S, Cheng L and Zhang L 2018 Ultralight MXene-coated, interconnected SiCnws three-dimensional lamellar foams for efficient microwave absorption in the X-band *ACS Appl. Mater. Interfaces* **10** 34524–33

[49] Shi S, Qian B, Wu X, Sun H, Wang H, Zhang H-B, Yu Z-Z and Russell T P 2019 Self-assembly of MXene-surfactants at liquid–liquid interfaces: from structured liquids to 3D aerogels *Angew. Chem., Int. Ed.* **58** 18171–6

[50] Wang L, Qiu H, Song P, Zhang Y, Lu Y, Liang C, Kong J, Chen L and Gu J 2019 3D $Ti_3C_2T_x$ MXene/C hybrid foam/epoxy nanocomposites with superior electromagnetic interference shielding performances and robust mechanical properties *Composites* A **123** 293–300

[51] Xu H, Yin X, Li X, Li M, Liang S, Zhang L and Cheng L 2019 Lightweight Ti_2CT_x MXene/poly(vinyl alcohol) composite foams for electromagnetic wave shielding with absorption-dominated feature *ACS Appl. Mater. Interfaces* **11** 10198–207

[52] Li R, Ding L, Gao Q, Zhang H, Zeng D, Zhao B, Fan B and Zhang R 2021 Tuning of anisotropic electrical conductivity and enhancement of EMI shielding of polymer composite foam via CO_2-assisted delamination and orientation of MXene *Chem. Eng. J.* **415** 128930

[53] Liu J, Zhang H-B, Sun R, Liu Y, Liu Z, Zhou A and Yu Z-Z 2017 Hydrophobic, flexible, and lightweight MXene foams

for high-performance electromagnetic-interference shielding *Adv. Mater.* **29** 1702367

[54] Yang Y-D, Liu G-X, Wei Y-C, Liao S and Luo M-C 2021 Natural rubber latex/MXene foam with robust and multifunctional properties %J *e-Polymers* **21** 179–85

[55] Jia X, Shen B, Zhang L and Zheng W 2021 Construction of compressible polymer/MXene composite foams for high-performance absorption-dominated electromagnetic shielding with ultra-low reflectivity *Carbon* **173** 932–40

[56] Lin B *et al* 2020 MXene/chitosan nanocoating for flexible polyurethane foam towards remarkable fire hazards reductions *J. Hazard. Mater.* **381** 120952

[57] Ma W, Cai W, Chen W, Liu P, Wang J and Liu Z 2021 A novel structural design of shielding capsule to prepare high-performance and self-healing MXene-based sponge for ultra-efficient electromagnetic interference shielding *Chem. Eng. J.* **426** 130729

[58] Sang M, Wu Y, Liu S, Bai L, Wang S, Jiang W, Gong X and Xuan S 2021 Flexible and lightweight melamine sponge/MXene/polyborosiloxane (MSMP) hybrid structure for high-performance electromagnetic interference shielding and anti-impact safe-guarding *Composites* B **211** 108669

[59] Shi H *et al* 2020 3D flexible, conductive, and recyclable $Ti_3C_2T_x$ MXene-melamine foam for high-areal-capacity and long-lifetime alkali-metal anode *ACS Nano* **14** 8678–88

[60] Yuan W, Liu H, Wang X, Huang L, Yin F and Yuan Y 2021 Conductive MXene/melamine sponge combined with 3D printing resin base prepared as an electromagnetic interferences shielding switch *Composites* A **143** 106238

[61] Zeng Z-H, Wu N, Wei J-J, Yang Y-F, Wu T-T, Li B, Hauser S B, Yang W-D, Liu J-R and Zhao S-Y 2022 Porous and ultra-flexible crosslinked MXene/polyimide composites for multifunctional electromagnetic interference shielding *Nano-Micro Lett.* **14** 59

[62] Bian R, Lin R, Wang G, Lu G, Zhi W, Xiang S, Wang T, Clegg P S, Cai D and Huang W 2018 3D assembly of Ti_3C_2-MXene directed by water/oil interfaces *Nanoscale* **10** 3621–5

[63] Fan Q, Yi M, Chai C, Li W, Qi P, Wang J and Hao J 2022 Oxidation stability enhanced MXene-based porous materials derived from water-in-ionic liquid pickering emulsions for wearable piezoresistive sensor and oil/water separation applications *J. Colloid Interface Sci.* **618** 311–21

[64] Zheng Z, Zhao Y, Ye Z, Hu J and Wang H 2022 Electrically conductive porous MXene-polymer composites with ultralow percolation threshold via pickering high internal phase emulsion templating strategy *J. Colloid Interface Sci.* **618** 290–9

[65] Cao H, Escamilla M, Arole K D, Holta D, Lutkenhaus J L, Radovic M, Green M J and Pentzer E B 2021 Flocculation of MXenes and their use as 2D particle surfactants for capsule formation *Langmuir* **37** 2649–57

[66] Shah S A, Habib T, Gao H, Gao P, Sun W, Green M J and Radovic M 2017 Template-free 3D titanium carbide ($Ti_3C_2T_x$) MXene particles crumpled by capillary forces *Chem. Commun.* **53** 400–3

[67] Zhao X *et al* 2020 pH, nanosheet concentration, and antioxidant affect the oxidation of $Ti_3C_2T_x$ and Ti_2CT_x MXene dispersions *Adv. Mater. Interfaces* **7** 2000845

[68] Zhao X, Holta D E, Tan Z, Oh J-H, Echols I J, Anas M, Cao H, Lutkenhaus J L, Radovic M and Green M J 2020 Annealed $Ti_3C_2T_z$ MXene films for oxidation-resistant functional coatings *ACS Appl. Nano Mater.* **3** 10578–85

[69] Rozmysłowska-Wojciechowska A, Karwowska E, Gloc M, Woźniak J, Petrus M, Przybyszewski B, Wojciechowski T and Jastrzębska A M 2020 Controlling the porosity and biocidal properties of the chitosan-hyaluronate matrix hydrogel nanocomposites by the addition of 2D $Ti_3C_2T_x$ MXene *Materials* **13** 4587

[70] Zhang Y-Z, El-Demellawi J K, Jiang Q, Ge G, Liang H, Lee K, Dong X and Alshareef H N 2020 MXene hydrogels: fundamentals and applications *Chem. Soc. Rev.* **49** 7229–51

[71] Zhou S, Bismarck A and Steinke J H G 2012 Interconnected macroporous glycidyl methacrylate-grafted dextran hydrogels synthesised from hydroxyapatite nanoparticle stabilised high internal phase emulsion templates *J. Mater. Chem.* **22** 18824–9

[72] Luo Q, Wang Y, Yoo E, Wei P and Pentzer E 2018 Ionic liquid-containing pickering emulsions stabilized by graphene oxide-based surfactants *Langmuir* **34** 10114–22

[73] Zhao X *et al* 2019 Antioxidants unlock shelf-stable $Ti_3C_2T_x$ (MXene) nanosheet dispersions *Matter* **1** 513–26

[74] Aghaei S M, Torres I, Baboukani A R, Khakpour I and Wang C 2019 Impact of surface oxidation on the structural, electronic transport, and optical properties of two-dimensional titanium nitride (Ti_3N_2) MXene *Comput. Condens. Matter* **20** e00382

[75] Fu X, Yang Q and Zhang Y 2021 Thermal decomposition behavior and mechanism study of cationic polyacrylamide *J. Therm. Anal. Calorimetry* **146** 1371–81

[76] Yang M-H 1998 The two-stages thermal degradation of polyacrylamide *Polym. Test.* **17** 191–8

[77] Naguib M, Saito T, Lai S, Rager M S, Aytug T, Parans Paranthaman M, Zhao M-Q and Gogotsi Y 2016 $Ti_3C_2T_x$ (MXene)–polyacrylamide nanocomposite films *RSC Adv.* **6** 72069–73

[78] Luo J-Q, Zhao S, Zhang H-B, Deng Z, Li L and Yu Z-Z 2019 Flexible, stretchable and electrically conductive MXene/natural rubber nanocomposite films for efficient electromagnetic interference shielding *Compos. Sci. Technol.* **182** 107754

[79] Habib T, Zhao X, Shah S A, Chen Y, Sun W, An H, Lutkenhaus J L, Radovic M and Green M J 2019 Oxidation stability of $Ti_3C_2T_x$ MXene nanosheets in solvents and composite films *npj 2D Mater. Appl.* **3** 8

[80] Arole K, Blivin J W, Saha S, Holta D E, Zhao X, Sarmah A, Cao H, Radovic M, Lutkenhaus J L and Green M J 2021 Water-dispersible $Ti_3C_2T_z$ MXene nanosheets by molten salt etching *iScience* **24** 103403